

C_{60}^+ - looking for the bucky-ball in interstellar space

G.A. Galazutdinov^{1,2,3,*}, V.V. Shimansky⁴, A. Bondar⁵, G. Valyavin³, J. Krelowski⁶

¹*Instituto de Astronomia, Universidad Catolica del Norte, Av. Angamos 0610, Antofagasta, Chile*

²*Pulkovo Observatory, Pulkovskoe Shosse 65, Saint-Petersburg 196140, Russia*

³*Special Astrophysical Observatory, Nizhnij Arkhyz, 369167, Russia*

⁴*Kazan Federal University, Kazan, 420008, Russia*

⁵*International Center for Astronomical and Medico-Ecological Research, Zabolotnoho Str. 27, Kiev, 03187, Ukraine*

⁶*Center for Astronomy, Nicholas Copernicus University, Gagarina 11, Pl-87-100 Torun, Poland*

Accepted XXX. Received YYY; in original form ZZZ

ABSTRACT

The laboratory gas phase spectrum recently published by Campbell et al. has reinvigorated attempts to confirm the presence of the C_{60}^+ cation in the interstellar medium, thorough an analysis of the spectra of hot, reddened stars. This search is hindered by at least two issues that need to be addressed: (i) the wavelength range of interest is severely polluted by strong water- vapour lines coming from the Earth's atmosphere; (ii) one of the major bands attributed to C_{60}^+ , at 9633 Å, is blended with the stellar MgII line, which is susceptible to non-local-thermodynamic equilibrium effects in hot stellar atmospheres. Both these issues are here carefully considered here for the first time, based on high-resolution and high signal-to-noise ratio echellé spectra for 19 lines of sight. The result is that the presence of C_{60}^+ in interstellar clouds is brought into question.

Key words: ISM: clouds - ISM: lines and bands - ISM: molecules

1 INTRODUCTION

One of the carbon allotropes, the spherical fullerene molecule C_{60}^+ (buckminsterfullerene, bucky-ball) is of particular interest for astrophysics. Indeed, in their seminal paper presenting the discovery of C_{60}^+ (Kroto et al., 1985), authors suggested that the molecule might give rise to a super stable species which might exist in interstellar space and circumstellar shells. A decade later, the first attempt to find C_{60}^+ in interstellar medium was made by Foing & Ehrenfreund (1994), who reported on the detection of two interstellar absorptions, at 9577 and 9633 Å, almost coincident with the wavelengths expected for C_{60}^+ . However, the limited number of observed sight lines, and the fact that the laboratory spectra were acquired in solid state matrices, made that identification uncertain. Jenniskens et al. (1997) and Galazutdinov et al. (2000) pointed out two difficulties inherent to the search for interstellar C_{60}^+ (see the Abstract above), and mentioned the non-detection of minor C_{60}^+ bands, expected at 9429 and 9366 Å (telluric lines are particularly strong in this wavelength range). Galazutdinov et al. (2000) also presented the first, simplified attempt to eliminate the influence of stellar MgII line.

In 2010 Cami et al. reported on the first detection of infrared emissions carried by neutral C_{60} seemingly attached

to the solid material (dust particles). These emissions were observed in the vicinity of a peculiar planetary nebula Tc1. Independently, Sellgren et al. (2010) reported on the presence of neutral C_{60} in the NGC 7023 reflection nebula illuminated by a B star HD 200775. The same nebula was recently identified as a source of C_{60}^+ , following the discovery of emission bands at 6.4, 7.1, 8.2, and 10.5 μm by Berné et al. (2013). The molecule was detected only in the regions closest to the star. All these reports fostered the hope that the buckminsterfullerene cation would be detected in translucent interstellar clouds. However, the laboratory spectra of C_{60}^+ , available in 1994, were measured for a solid medium (cryogenic matrix), and these spectra therefore could not offer any firm confirmation of this ion as the one responsible for known 9577 and 9633 Å diffuse bands.

The dormant interest in discovering interstellar bucky-ball cations was revived following the recent publication of laboratory gas-phase spectra by Campbell et al. (2015). According to the authors, C_{60}^+ exhibits four relatively strong spectral lines, centered at 9365.9 ± 0.1 , 9428.5 ± 0.1 , 9577.5 ± 0.1 and 9632.7 ± 0.1 Å, with relative intensities of 0.2, 0.3, 1.0 and 0.8 respectively. New attempts to confirm the presence of this molecule in the interstellar medium, by analysing the spectra of hot, reddened stars, were recently reported by Walker et al. (2015), who have also tried to detect the two weaker spectral features of C_{60}^+ in the sight lines towards HD 183143 and HD 169454. Very recently, Camp-

* E-mail: runizag@gmail.com

bell, Holz & Maier (2016) reported on the detection of a very weak feature at 9348.5 Å (just 1/10 of the intensity of the major 9577 Å band), again in a spectrum of HD 183143. Unfortunately, both these studies lack an analysis of possible pollution by telluric lines. Indeed, as we demonstrate below, the DIB9633 in both HD 169454 and HD 183143 spectra significantly contaminated by stellar MgII 9632 Å line. Generally, the HD 183143 sight line is not a good choice for finding any new diffuse bands. As demonstrated in the respective DIB surveys (Galazutdinov et al. 2000b, Hobbs et al. 2009), it is often not easy to distinguish between stellar and interstellar lines towards this relatively cool and slowly rotating white hypergiant classified as B6 to B8 Ia-0 (Chentsov 2004).

Here we present the most careful analysis to date of near-infrared interstellar features commonly attributed to C_{60}^+ , for a relatively large sample of targets. We took into account the possibilities of spectral contamination not only from telluric but also from stellar lines. Indeed, incidental overlap with stellar lines is at particularly important danger in cases such as HD 183143, where broad interstellar features have widths comparable to the stellar lines, the latter being numerous in this late B type supergiant.

2 SPECTRAL DATA

Our sample of astronomical data includes precise measurements of the 9577 Å and 9633 Å bands, the two major interstellar features allegedly resulting from C_{60}^+ . High signal-to-noise and high resolution echellé spectra were obtained for 19 heavily reddened targets (Tables 1 and 2) with the UVES spectrograph fed by the Kueyen 8-m telescope at Paranal. The resolving power $R = \lambda/\Delta\lambda$ was 80,000 in the range of MgII 4481.2 Å line, and 110,000 in the range of currently analysed diffuse interstellar bands (DIB).

All spectra were processed and measured in a standard way using both IRAF (Tody 1986) and our own DECH¹ codes. The wavelength scale of all spectra was corrected by well-known atomic/molecular interstellar lines, e.g. K1 and C₂.

2.1 Telluric contamination

Near infrared wavelength range, when observed using ground-based instruments, is subject to strong contamination by telluric lines. In order to eliminate them, we applied the classical method implemented based on the use of a divisor, namely the spectrum of an unreddened, hot, and preferably rapidly rotating, star. Our software allowed for the compensation of both positional and intensity variability within the set of observed telluric lines. As a divisor we used the UVES spectra of Spica (HD 116658). Recently, Tkachenko et al. (2016) published an extensive study of this close binary system, which has an orbital period of $\sim 4^d$, effective temperatures of $25,300 \pm 500$ K and $20,900 \pm 500$ K, logarithms of gravity 3.71 ± 0.10 and 4.15 ± 0.15 , rotational velocities $v \sin i$ 165.3 ± 4.5 km/s and 58.8 ± 1.5 km/s, for the primary and secondary components respectively. When used for the removal of telluric lines, the complex and variable spectrum

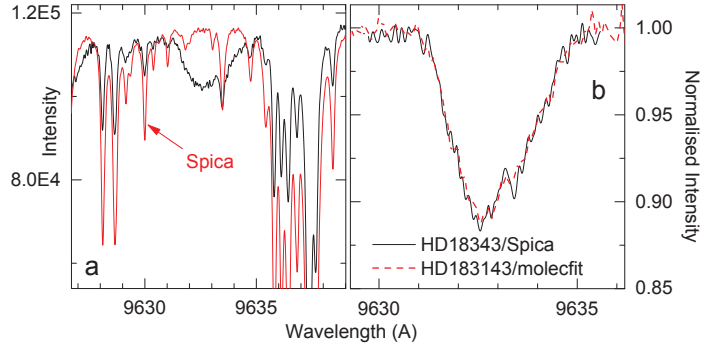


Figure 1. a) Spectra of HD 183143 and Spica in the vicinity of DIB9633. b) Comparison of DIB9633 profiles after the removal of telluric lines using Spica and MOLECFIT.

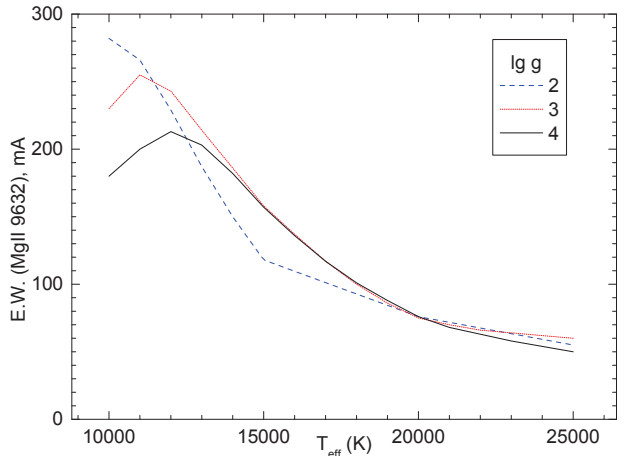


Figure 2. Variation of the non-LTE equivalent width of MgII 9632 Å line with the change of stellar parameters. Note that model spectra are calculated assuming the solar chemical composition and a fixed microturbulent velocity value, 5 km/s. In general, microturbulent velocity grows with temperature rise and with decrease of gravity.

of Spica may introduce unwanted distortion into relatively broad profiles, such as that of DIB9633, owing to the presence of stellar line(s). This is depicted in Figure 1a for the DIB9633 profile observed towards HD 183143. The lack of a stellar, contaminating component inside the DIB9633 profile, is evident. However, in order to check for the applicability of Spica's spectra as divisors, we tested the recently introduced MOLECFIT procedure (Smette et al., 2015), a software tool designed to remove atmospheric absorption features. Fig. 1b shows a good matching of the DIB9633 profiles derived with the divisor (Spica) and MOLECFIT approaches. The same quality of agreement has also been found for the other three bands that are candidates for C_{60}^+ absorptions. We checked the removal of telluric lines for all targets using both methods.

3 MGII CONTAMINATION

Background stars are obviously not ideal sources of radiation for measuring interstellar absorptions, particularly because of the presence of their own spectral features. The pollution

¹ <http://gazinur.com/DECH-software.html>

Table 1. Basic parameters of the observed stars. Effective temperature - T_{eff} (K), logarithm of gravity - $\lg g$ ($cm s^{-2}$), microturbulent velocity - v_{turb} ($km s^{-1}$), projected rotational velocity - $v \sin i$ ($km s^{-1}$), abundances of marked chemical elements relative to the solar abundance - $[X/H]$ (dex).

Star	T_{eff}	$\lg g$	v_{turb}	$v \sin i$	Abundance $[X/H]$								
					He	C	N	O	Fe	Si	Mg	Al	Ne
CD-324348	19,500	2.45	9	36	+0.30	-0.30	+0.30	-0.30	-0.20	+0.50	+0.30	-0.30	+0.20
BD-145037	18,000	1.80	10	42	+0.30	+0.10	+0.30	+0.10	+0.20	+0.30	+0.10	+0.20	
HD 23180	24,000	3.45	13	78	+0.15	-0.10	-0.20	-0.10	-0.20	-0.40	-0.25		
HD 27778	15,500	3.80	5	92	+0.20	-0.05	-0.20	+0.05	-0.40	-0.40	-0.50		
HD 63804*	9,400?	1.10?	6?	?	+0.15:	-0.20:			-0.20:		-0.30:		
HD 76341	34,000	3.70	13	66	+0.25	+0.20	+0.40	+0.20		+0.40	-0.05	-0.10	+0.20
HD 78344	31,000	3.30	13	98	+0.30	+0.30	+0.50	+0.30		+0.50	+0.10	+0.10	+0.30
HD 80077	17,000	2.00	15	47	+0.05	-0.40	+0.40	+0.10	+0.10	+0.40	-0.05	+0.10	
HD136239	17,000	1.80	11	43	+0.40	+0.30	+0.50	+0.30	+0.20	+0.50	+0.30	+0.20	
HD145502	21,000	4.00	8	98	-0.10	-0.70	+0.40	+0.05	-0.20	+0.15	-0.60		
HD147888	16,000	4.10	5	104	-0.10	-0.10	-0.10	+0.00	-0.30	-0.10	-0.50		
HD148379	17,000	1.70	14	51	+0.30	-0.10	+0.30	+0.10	+0.10	+0.20	+0.10	+0.00	
HD148605	20,500	4.20	11	145	+0.15	-0.30	-0.40	-0.30	-0.60	-0.60	-0.60		
HD167264	29,000	3.20	16	82	+0.35	+0.10	+0.30	+0.25	-0.20	-0.10	+0.00		
HD168625	14,000	2.00	10	52	+0.00	-0.20	+0.25	-0.05	-0.10	+0.05	+0.05	+0.00	
HD169454	21,000	2.10	16	39	+0.10	+0.30	+0.50	+0.30		+0.60	+0.30	+0.20	+0.20
HD170740	21,000	3.90	10	40	+0.00	-0.05	-0.15	-0.20	-0.40	-0.40	-0.45		
HD183143	11,500	1.40	8	37	+0.00	+0.00	+0.30	+0.10	-0.20	+0.10	+0.10		
HD184915	27,000	3.40	19	220	+0.30	+0.10	+0.50	+0.00		-0.10	+0.00		

* - see the comment in "MgII contamination" section.

Table 2. Measurements of four C_{60}^+ candidate bands. Upper, cumulative column captions give: laboratory central wavelength, laboratory full width at half maximum (FWHM), and laboratory intensity normalized to the strength of the 9577 Å band - $(I/I_{9577})_{lab}$ (Campbell et al., 2015). The lower captions give: observed central wavelength (Å), observed equivalent widths (mÅ), observed FWHM, and intensity normalized to that of the 9577 Å feature. Two equivalent width values are given for the 9633 Å band: EW_o (before correction) and EW_c (after the removal of the MgII blending feature). Measurement errors are given in parentheses.

Continued...

Star	9632.7(0.1), 2.2(0.2), $(I/I_{9577})_{lab}=0.8$					9577.5(0.1), 2.5(0.2), $I_{lab}=1.0$		
	λ_c	EW_o (mÅ)	EW_c (mÅ)	FWHM(Å)	I/I_{9577}	λ_c	EW_o (mÅ)	FWHM(Å)
CD-32 4348	9632.2 (0.1)	173(17)	75(16)	2.1(0.1)	0.4	9576.9(0.2)	168(11)	3.0(0.3)
BD-14 5037	9632.5 (0.1)	202(20)	125(15)	2.9(0.3)	1.2	9577.1(0.2)	107(10)	2.8(0.2)
HD 23180	9633.1 (0.2)	145(40)	141(46)	3.7(0.3)	1.8	9577.5(0.2)	77(34)	3.6(0.3)
HD 27778	9632.6 (0.2)	94(22)	64(17)	2.7(0.2)	1.3	9577.5(0.2)	50(30)	2.2(0.3)
HD 63804*	9632.2 (0.3)	150(24)	20(20)	2.7(0.3)	0.1	9576.9(0.1)	207(11)	
HD 76341	9632.2 (0.2)	136(30)	134(30)	2.5(0.2)	1.2	9577.2(0.2)	110(20)	2.5(0.2)
HD 78344	9632.3 (0.2)	170(13)	170(13)	2.9(0.2)	0.6	9576.9(0.2)	294(15)	3.7(0.3)
HD 80077	9632.15(0.15)	168(14)	95(11)	2.0(0.2)	0.6	9577.3(0.1)	160(10)	2.9(0.2)
HD136239	9631.8 (0.1)	252(25)	120(20)	2.4(0.2)	0.6	9576.9(0.2)	195(15)	2.9(0.2)
HD145502	9632.3 (0.2)	160(20)	158(20)	3.1(0.2)	1.3	9576.9(0.2)	120(30)	3.5(0.3)
HD147888	9632.2 (0.2)	175(11)	110(12)	3.2(0.2)	1.6	9576.9(0.2)	70(20)	3.3(0.3)
HD148379	9632.2 (0.2)	182(11)	80(11)	2.4(0.2)	0.6	9577.3(0.2)	137(9)	3.3(0.2)
HD148605	9632.25(0.1)	120(30)	119(35)	3.4(0.2)	1.5	9576.9(0.2)	80(20)	3.7(0.4)
HD167264	9632.4 (0.2)	88(18)	82(20)	2.7(0.2)	1.4	9576.8(0.2)	60(17)	3.2(0.2)
HD168625	9631.5 (0.1)	342(26)	194(25)	1.8(0.1)	0.6	9576.2(0.1)	320(25)	3.1(0.2)
HD169454	9631.4 (0.3)	210(25)	130(20)	2.7(0.2)	1.6	9577.1(0.1)	82(10)	2.3(0.2)
HD170740	9632.1 (0.2)	175(20)	150(20)	2.8(0.1)	1.6	9576.9(0.2)	93(20)	3.0(0.4)
HD183143	9632.5 (0.2)	230(20)	105(20)	1.9(0.3)	0.4	9577.3(0.2)	300(20)	2.9(0.2)
HD184915	9632.4 (0.3)	71(25)	70(25)	2.5(0.1)	1.0	9576.9(0.2)	70(20)	3.5(0.3)

* - The corrected equivalent width of DIB9633 measured towards HD 63804 is an upper limit, owing to uncertain basic stellar parameters.

Table 2 – *continued*.

Star	9428.5(0.1), 2.4(0.1), (I/I ₉₅₇₇) _{lab} =0.3				9365.9(0.1), 2.4(0.1), (I/I ₉₅₇₇) _{lab} =0.2			
	λ_c	EW _o (mÅ)	FWHM(Å)	I/I ₉₅₇₇	λ_c	EW _o (mÅ)	FWHM(Å)	I/I ₉₅₇₇
CD-32 4348	n/a	<5		<0.1		n/a		
BD-14 5037		strong telluric			9365.4(0.3)	30(30)	2.2(0.2)	0.15
HD 23180		n/a				n/a		
HD 27778		n/a				<50		<1
HD 63804		n/a				n/a		
HD 76341		n/a				<30(30)		<0.3
HD 78344		<2(2)		<0.01		<30830)		<0.1
HD 80077	9428.15(0.1)	50(50)	2.5(0.5)	0.3	9365.5(0.3)	50(50)	2.5(0.5)	0.3
HD136239		strong telluric				strong telluric		
HD145502		n/a				n/a		
HD147888		n/a				n/a		
HD148379		n/a			9365.7(0.3)	38(25)	2.6(0.3)	0.2
HD148605		n/a				n/a		
HD167264		n/a				n/a		
HD168625		n/a				<60		<0.25
HD169454		n/a				strong telluric		
HD170740		n/a				n/a		
HD183143		<50		<0.1		strong telluric		
HD184915		n/a				n/a		

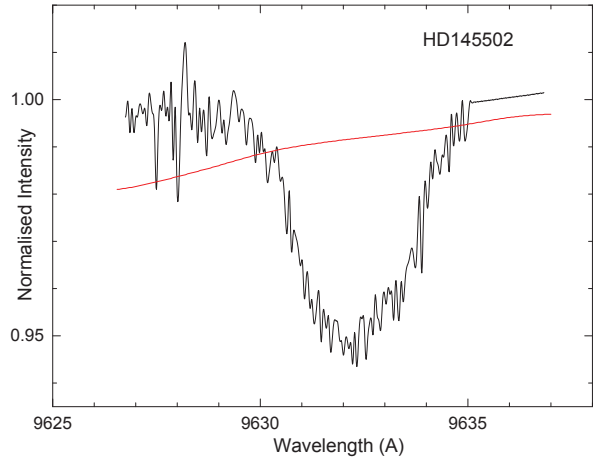
Table 3. Oscillator strength of 4481 and 9632 Å MgII triplets.

λ (Å)	lg gf	λ (Å)	lg gf
4481.1260	0.74	9631.8910	0.59
4481.1500	-0.56	9631.9470	-0.71
4481.3250	0.59	9632.4300	0.43

of the DIB9633 profile by the stellar MgII line, even though it has been discussed in the past, has never been properly taken into account. Estimations of MgII 9632 Å line strengths are complicated by the sensitivity to non-local thermodynamic equilibrium (non-LTE) effects present in atmospheres of hot stars. The variability of this atomic feature with changing stellar parameters (for solar chemical composition only) is shown in Fig. 2. However, we caution against a simplified conclusion that the removal of the MgII 9632 Å line is always compulsory. For the majority of hot objects the line is in fact weak, shallow, and much broader than DIB9633, owing to the rapid rotation and/or high gravity (e.g. HD 145502, see Table 1), so that it may not noticeably alter the coinciding DIB profile (see Fig 3).

There are particular “lucky” instances where the blend of DIB9633 and MgII can be easily resolved. This may occur when the difference between the radial velocity of a background star and the velocity of the studied interstellar cloud is large or when the DIB is intrinsically shifted in relation to its “normal” positions. HD 37022 offers the example of this latter possibility (Fig. 4) with the red-shift of DIB9633 discovered by Krelowski & Greenberg (1999) and recently confirmed by Krelowski et al. (2015). On the other hand, even an evidently strong stellar line may hide completely inside the DIB profile when the radial velocities of a star and the cloud are similar (Fig. 4).

The stellar line of ionized magnesium can thus in many cases severely contaminate the DIB9633 profile. In order to eliminate this effect, we first corrected the oscillator strength

**Figure 3.** DIB9633 profile, as observed towards HD 145502, after the telluric correction (the corresponding fragment of synthetic stellar spectrum is shown in red). This exemplifies the case of no detectable MgII effect.

(gf) of the MgII 9632.1 Å transition, using a high quality UVES spectrum of Sirius, where both neutral and ionized magnesium lines are easily seen. The magnesium abundance was estimated based on the well-known lines at 4703.0, 5183.6, 5528.4 Å (MgI) and 4481.2 Å (MgII) measured in the spectrum of Sirius. Then, the oscillator strength of the 9632 Å MgII line (Table 3) was corrected by matching the observed profile with the model spectrum (Fig. 5).

The basic stellar parameters of the program stars (effective temperature, logarithm of gravity, rotational velocity, chemical composition) were determined with the aid of STAR code (Menzhevitski et al., 2014) which takes account of non-LTE effects for H I, He I, He II, C II, C III and Mg II species. Hydrostatic models of stellar atmospheres were calculated using the program ATLAS12 (Castelli & Kurucz, 2004), and the non-LTE populations for the above men-

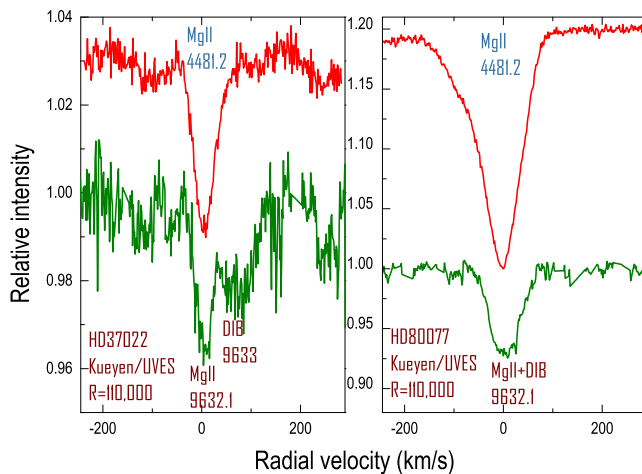


Figure 4. Stellar MgII 4481.2 Å line versus the DIB9633 profile, as plotted against the radial velocity scale. The presence of MgII 9632 Å line alongside the DIB is obvious for HD 37022. Conversely, both spectral features overlap perfectly in the case of HD 80077, so that the DIB is much weaker than it appears, and the separation of two contributions requires a careful procedure.

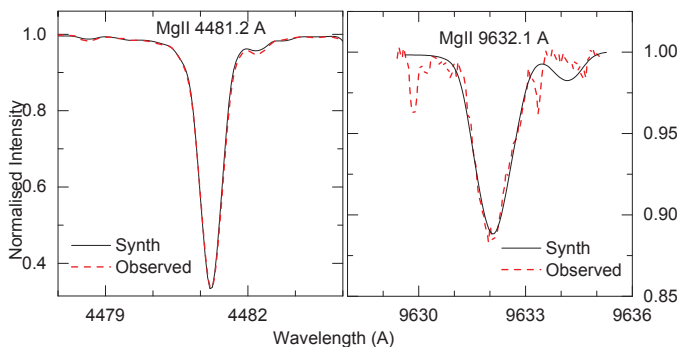


Figure 5. Profiles of MgII 4481.2 and 9632.1 Å lines in the spectrum of Sirius, shown with the corresponding synthetic spectrum. The corrected oscillator strengths are given in Tab. 3.

tioned elements were derived using the software package NONLTE3 (Sakhibullin, 1983).

The magnitude of non-LTE effects and chemical composition of the investigated stars were derived by the analysis of certain atomic lines located in wavelength ranges free of telluric contamination and having well-determined parameters, for example: H ϵ -H δ , HeI 4009.2, 4026.2, 4387.9, 4471.5, 4713.2, 4921.9, 5047.8 Å, HeII 4199.8, 4541.6 Å, CII 3918.9, 3920.8, 4266.9 Å, CIII 4651.5, 4665.9 Å, MgII 4481.2 Å.

The basic parameters of the observed stars and the derived abundance of several chemical elements are listed in Table 1. It is confirmed that subtraction of the stellar 9632 Å MgII line may essentially reduce the intensity of the interstellar feature at 9633 Å (Fig. 6). Conversely, DIB9577 is not polluted by stellar lines, for all the sight lines investigated here. Our results for the four DIBs previously assigned to C_{60}^+ are collected in Table 2. Note that equivalent widths of DIB9633 are given in two separate columns which list the

values without and with the correction for the stellar MgII line.

Below we provide information specific to each of the studied targets.

CD-32 4348 The abundance of alpha elements is $[x/H] = -0.4$ dex. Moderate deficits of helium, magnesium and nitrogen are revealed, while silicon exhibits an overabundance. A strong blend of MgII 4481 Å and AlIII 4479 Å lines generated in the model spectrum matches the observed profile well. Subtracting the 9632 Å line of MgII reduces the intensity of DIB9633 almost half. Minor bands at 9429 and 9366 Å, expected for C_{60}^+ are below the level of detection.

BD-14 5037 Overabundances of He, N, Si (up to +0.3 dex) are typical for stars experiencing the CNO-cycle. The magnesium abundance $[Mg/H] = 0.1$ dex is accurately estimated by means of the MgII 4481 Å line. This object provides an example of the diffuse band at 9633 Å being stronger than that at 9577 Å, despite that the intensity of former being reduced by the removal of the contribution from stellar magnesium.

HD 23180 There is a good coincidence of the observed phase of this binary target with the model spectrum. The magnitude of non-LTE effects is low. The chemical composition exhibits a small deficit of heavy elements. The binarity of the target is well seen in the observed spectrum but can be reproduced. The doubled profile of MgII 4481 Å line is satisfactorily coincident with the model spectrum. A weak MgII line at 9632 Å fades with strong HeI line to a smeared blend.

HD 27778 There is good coincidence of observed and model spectra. The magnitude of non-LTE effects is low. The chemical composition exhibits some underabundance of iron (a metallicity deficit is generally observed in this object), an excess of helium, and a noticeable irregularity in the abundances of heavy elements. The symmetric profile of 4481 Å MgII line is very well reproduced in the synthetic spectrum. The 9632 Å line of MgII makes a major contribution to a blend with DIB9633.

HD 63804 The basic stellar parameters of this object can be reliably determined based on H I Balmer lines and on the spectral features of HeI, FeI, FeII, CII, SiII. However, the observed MgII 4481 Å line is too strong, considering any realistic abundance of magnesium. Weaker MgI and MgII lines point to $[Mg/H] = -0.3$ dex. The star is probably a spectroscopic binary, with components having the effective temperature of ~ 8000 and ~ 14000 K. The cooler object is brighter, with its spectral lines red-shifted by ~ 40 -50 km/s. Additional spectra, acquired 1-2 years later, will permit for a more complete description. Nevertheless, a strong MgII 9632 Å line leaves little space for the interstellar 9633 Å feature. The latter has just 1/10 of the DIB9577 intensity, which is eight times weaker than expected assuming C_{60}^+ as the carrier. The lack of weaker 9429 and 9366 Å bands is obvious.

HD 76341 This object is very hot O-type giant. Helium, silicon and nitrogen are in similar excess of +0.2 dex. Broad stellar lines are not able to distort the discussed infrared DIBs. This sight line offers yet another example of DIB9633 being stronger than DIB9577, in contrast to the case for the laboratory gas phase spectrum of C_{60}^+ .

HD 78344 The chemical composition generally exhibits an overabundance of helium and light elements. Broad and

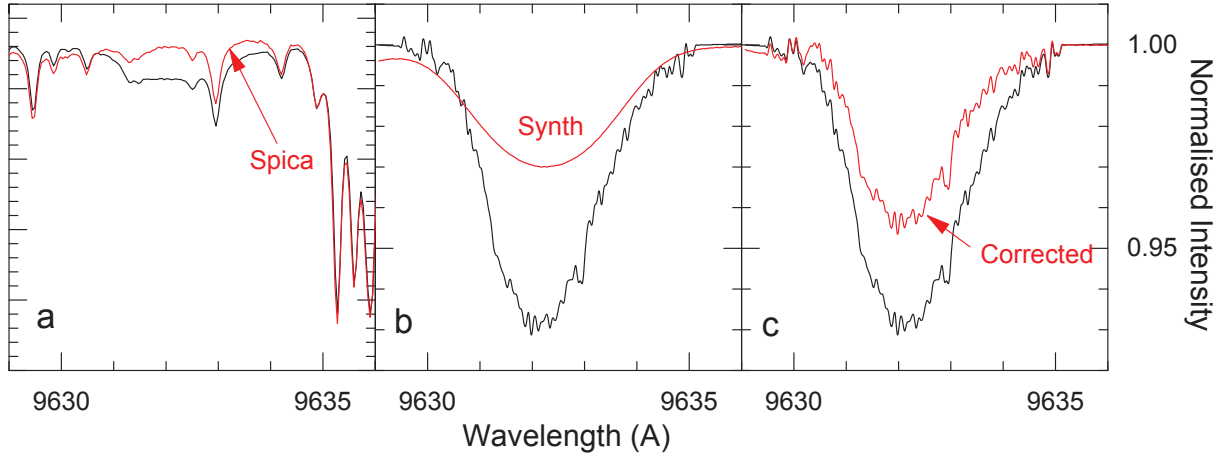


Figure 6. Consecutive stages of the DIB9633 profile correction, as illustrated for the HD 80077 sight line. **a)** Initial stage. Original spectrum, polluted by strong telluric lines, shown together with the spectrum of Spica, serving as the divisor; **b)** DIB profile with telluric lines removed (black). Smooth red curve represents the synthetic non-LTE profile of the stellar MgII 9632 line, derived with the parameters given in Tab. 1; **c)** Final stage. DIB9633 corrected for the presence of MgII line, shown together with the uncorrected profile.

shallow stellar lines do not affect the profiles of interstellar features. The DIB9633 intensity is just 0.6 of that found for DIB9577, instead of 0.8 expected with the assumption of C_{60}^+ as the carrier. The absence of weaker 9429 Å and 9366 Å bands is evident.

HD 80077 This star features a significant excess (~ 0.4 dex) of nitrogen, as well as of silicon, and a deficit of carbon of almost equal magnitude. Magnesium and helium abundances are almost solar. Other elements display an overabundance of ~ 0.1 dex. The MgII 9632 Å line is quite strong, which makes the true strength of DIB9633 a factor of 0.6 lower than that measured for DIB9577, instead of the value 0.8 anticipated assuming the assignments to C_{60}^+ . The presence or absence of weaker C_{60}^+ bands, at 9429 Å and 9366 Å, is doubtful owing to saturated telluric lines that significantly pollute that part of the spectrum.

HD136239 Excesses of +0.4 dex are found here for the alpha elements and helium. Nitrogen and silicon are overabundant by +0.5 dex. The stellar MgII line is strong, making the true intensity of DIB9633 half of expected assuming C_{60}^+ as the carrier. The presence/absence of 9429 Å and 9366 Å features is uncertain, owing to saturated telluric lines.

HD145502 There is only a moderate coincidence of observed and model spectra because of large differences of individual abundances for different lines of helium and carbon. The deficit of carbon and magnesium is anomalous. The MgII 4481 Å line has an irregular shape, and therefore cannot be well reproduced by our synthetic spectrum. The star is probably a binary object. A weak 9632 Å MgII line merges with strong HeI line to a smeared blend.

HD147888 A very good match with the model spectrum is observed. The magnitude of non-LTE effects is low. The chemical composition is characterized by smoothly decreasing elemental abundances for heavier species. Magnesium is evidently underabundant. The profile of MgII 4481 Å line, anomalous owing to strange, rather flat wings, is nevertheless well reproduced with the model. The MgII 9632 Å line makes a major contribution to the blend with DIB9633.

HD148379 The equivalent width of DIB9633 is reduced by almost a half after subtracting the coincident stellar mag-

nesium line. A weak feature is possibly present at 9366 Å but a strong telluric contamination prevents any precise measurements.

HD148605 There is a good coincidence of observed and model spectra. The magnitude of non-LTE effects is low. The chemical composition exhibits a smooth decrease of individual abundances of chemical elements for heavier species. The profile of the MgII 4481 Å line is symmetric, and well reproduced by the model. The weak 9632 Å MgII line merges with strong HeI line to a common smeared blend.

HD167264 Again, there is a good match of observed and model spectra. Line profiles are affected by the stellar wind. The spectral features of some light elements are perturbed by uncompensated non-LTE effects. There is a smooth decrease of individual elemental abundances for heavier species. The observed profile of MgII 4481 Å is very well reproduced by the model. There is no infrared MgII line polluting DIB9633.

HD168625 Here, the intensity of DIB9633 is substantially reduced after subtracting the contribution from MgII, which makes the equivalent widths ratio DIB9633/DIB9577 closer to that observed in laboratory gas phase spectra of C_{60}^+ .

HD169454 The object exhibits almost solar abundances of helium and magnesium, while nitrogen and silicon are in moderate excess. The synthetic profile of a blend made by MgII 4481 Å and AlIII 4479 Å matches the observed spectrum well. This sight line exemplifies the case of unusually strong 9633 Å band; even after the subtraction of the stellar MgII feature, the equivalent width is still higher than for DIB9577, in strong disagreement with the ratio of respective bands observed in the laboratory gas phase spectrum of C_{60}^+ .

HD170740 There is a reasonable coincidence of observed and model spectra in this binary object, with evident two-component profiles of HeI and CII. Stellar parameters were determined for the main component only. The chemical composition exhibits the deficit of metallicity, with a large scatter of abundances derived for different lines of helium and carbon. Both carbon and magnesium are in deficit. The observed profile of MgII 4481 Å is almost perfectly symmetric and clearly separated from the neighboring AlIII 4479 Å line,

as is very well reproduced by the synthetic spectrum. The intensity of DIB9633 is considerably reduced after the subtraction of the stellar MgII line contribution.

HD183143 There is a good coincidence of observed and model spectra. Hydrogen lines $H_\alpha - H_\delta$ exhibit strong, wind-driven emissions. The lines of other elements, including neutral helium, are symmetric and match the model. The chemical composition is almost solar, with a slight excess of nitrogen, probably as a result of the running CN-cycle. MgII 4481Å line has a symmetric profile, coincident with that generated in the synthetic spectrum. A contribution from the infrared MgII 9632 Å line, when subtracted, essentially reduces the intensity of DIB9633. HD 183143 is a key object for the recently announced detections of C_{60}^+ (Walker et al. 2015, Campbell et al. 2016). As noted, this identification of interstellar C_{60}^+ was premature, as it lacked the analysis of the stellar spectrum. Indeed, taking account of a considerable contribution from the stellar MgII line, the equivalent widths ratio DIB9633/DIB9577 is just 0.4.

HD184915 There is an excellent coincidence of observed and model spectra. Non-LTE effects are moderate, without any detectable stellar wind effects. The estimated rotational velocity is as high as 220 km/s. The chemical composition exhibits an excessive abundance of helium and nitrogen, probably owing to the enrichment of stellar surface by CNO-cycle products. The profile of the MgII 4481Å line is symmetric, which is well reproduced by the model. There is no MgII line overlapping DIB9633.

4 OBSERVED DIFFUSE BANDS VERSUS THE C_{60}^+ LABORATORY GAS PHASE SPECTRUM

The laboratory gas-phase absorption spectrum of C_{60}^+ features four main infrared bands: 9632.7, 9577.5, 9428.5 and 9365.9 Å (± 0.1 Å), with relative intensities of 0.8, 1.0, 0.3, and 0.2, respectively; thus the strongest peak is at 9577.5 Å (Campbell et al., 2015). No lines of sight in our sample allowed the detection of that spectral pattern. In particular, no candidates for the two weakest of the above listed bands have emerged (cf. the second part of Table 2).

Apart from that, the assignment of diffuse bands at 9633 Å and 9577 Å to the two strongest C_{60}^+ bands suffers from the fact that the observed intensity ratio DIB9633/DIB9577 varies greatly from target to target instead of scattering, within the known error limits, around a "canonical" value of 0.8 (see Tab. 2). Towards the majority of our targets, the 9633 Å band was in fact stronger than that at 9577 Å. On the other hand, lines of sight with extremely low DIB9633 intensities were revealed (Tab. 2). Such large variations of the observed strength ratio cast serious doubts on whether the two bands could indeed share a common carrier.

A convincing illustration of these issues is provided by the results acquired for HD 145502, an object free from the MgII effect and intentionally selected to waive all speculation concerning the accuracy of our stellar line removal procedure. Moreover, the elimination of telluric lines was particularly successful for HD 145502 (Fig. 7). For that sight line, DIB9633 is exceptionally strong, in fact much stronger than DIB9577, making the DIB9633/DIB9577 ratio as big as 1.3, instead of the 0.8 observed in laboratory gas-phase spectra.

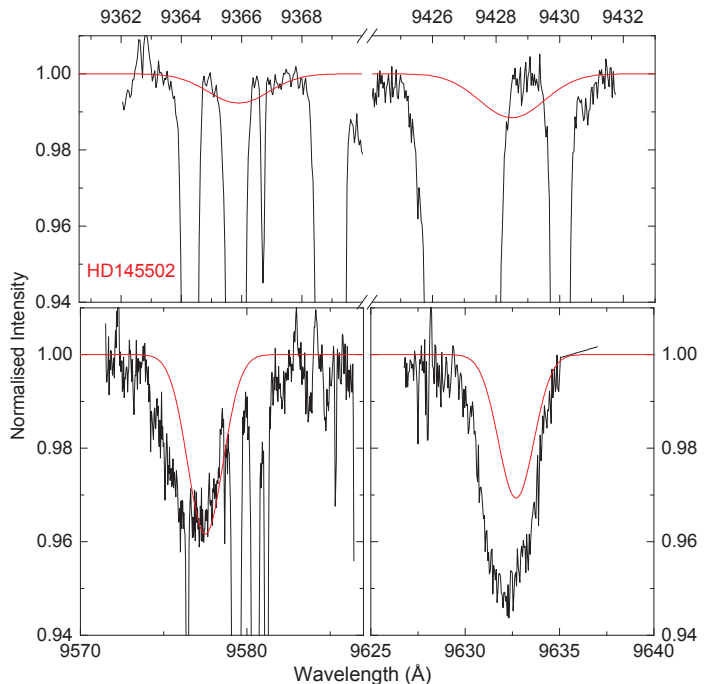


Figure 7. Observed near infrared spectrum of HD 145502. Smooth gaussian curves mimic the laboratory gas-phase bands of C_{60}^+ , with wavelengths, widths, and intensity ratios (normalized to the depth of DIB9577) taken from the Campbell et al. (2016) study. See text for details.

Both features are blue-shifted and broader than expected, when compared with the known C_{60}^+ bands. Concerning the two remaining, minor bands of C_{60}^+ , it is the case that the relevant wavelength range is very difficult to study because of exceptionally strong telluric lines, which are difficult to remove because of saturation effects. Nevertheless, the upper panel of Fig. 7 clearly demonstrates that there is no room for broad and shallow features of the expected depth. The Gaussians, normalized to the depth of DIB9577, intersect the observed spectrum making thus the presence of both weak features very unlikely.

The second example illustrates the opposite case, with a very small DIB9633/DIB9577 ratio. Indeed, in the spectrum of HD 183143, after the MgII correction, the intensity of DIB9633 was reduced by a factor of more than 2. The presence or absence of weak DIB9366 cannot be confirmed owing to very strong telluric lines which seem to be partially blended. The profile of another weak band, DIB9428, intersects the observed spectrum in which it can hardly be traced.

Another interesting object is HD37022. As depicted by Fig. 4, DIB9633 is red-shifted in this spectrum, similar to what was reported for DIB5780 (Krelowski et al. 2015). This leads to the spectral separation of DIB9633 from the MgII 9632 Å line. It is the only such case in our sample. Importantly, however, the other crucial C_{60}^+ candidate band, DIB9577, which is very broad in this spectrum, does *not* show any red-shift (and may even be slightly blue-shifted). This is further evidence against a common origin of the two major DIBs attributed to C_{60}^+ .

Very recently Campbell et al. (2016a) have corrected

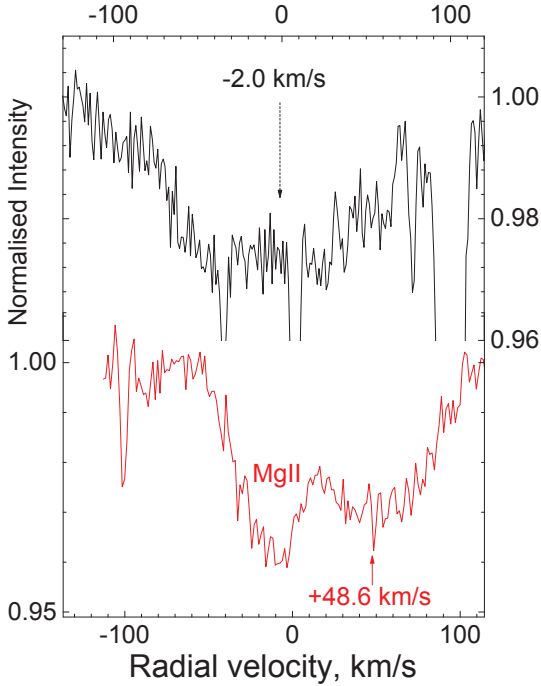


Figure 8. Radial velocity profiles for DIB9577 and DIB9633 observed towards HD 37022 made with “new” laboratory wavelength from Campbell et al. (2016a). The rest wavelength velocity scale was established using the interstellar K_I 7699 Å line.

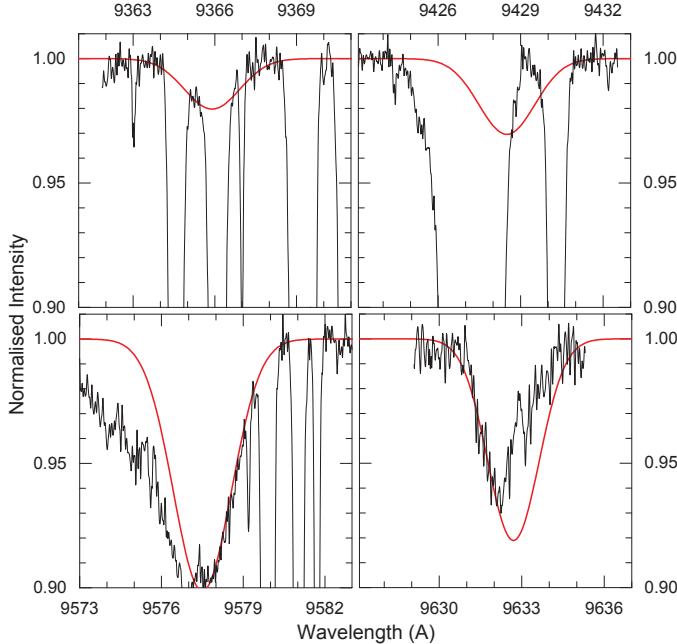


Figure 9. Same as Fig. 7, for HD 183143.

laboratory C_{60}^+ wavelengths, taking into account the fact that their previously reported values (Campbell et al. 2016) concerned weakly bound $C_{60}^+-He_n$ ($n = 1 - 3$) complexes. The absorption bands of such species exhibit progressive red-shifts with the increasing number of interacting He atoms (see figs 1 and 2 in Campbell et al., 2016a). Wavelengths estimations for bare C_{60}^+ cations were based on the linear

interpolation of measurements made for the complexes containing 1, 2 and 3 He atoms. Of note is the fact that the corrected wavelengths derived for the 2 major peaks of bare C_{60}^+ (9577.0 and 9632.1 Å, with ± 0.2 Å as the 2σ uncertainty) are in good agreement with the **mean** values calculated for our present sample of targets: 9577.0 and 9632.2 Å. However, the observed scatter of position of peaks in astronomical spectra greatly exceeds the uncertainty of measurements. Diffuse bands of the common origin have to be displaced in unison, keeping the same distance between them; in other words, the scatter of positions of diffuse bands in astronomical measurements (Table 2) cannot be explained by an assumption of their common origin. Indeed, as we already reported, DIB9633 and stellar MgII line at 9632 Å can be easily distinguished in the spectrum of HD 37022 (Fig. 4) where DIB9633 exhibits an evident red-shift, while the second major band 9577 fits the “new” lab wavelength well (Fig. 8). Note that in Fig. 8 both radial velocity profiles were constructed using the “new” rest wavelengths from Campbell et al. (2016a).

Interestingly, it is not the “new”, but rather “old” (i.e. uncorrected for the He complexes) laboratory position of the strongest C_{60}^+ band at 9577.5 ± 0.1 Å that matches well the DIB9577 wavelength 9577.4 ± 0.02 Å observed towards HD 183143 (both values are from Table 1 of Campbell et al., 2016). Our observations of HD 183143 (our Table 2) confirm the wavelength of interstellar feature at 9577 Å. Thus, there is surprising difference of 0.4-0.5 Å between the “new” laboratory wavelength and that observed in HD 183143.

Weak interactions between C_{60}^+ cations and some common constituents of the interstellar gas remain to be modelled and/or measured in laboratories. At present it’s anybody’s guess that such complexes, if bound strong enough to withstand the temperatures of the translucent interstellar medium, would have spectra differing from that of bare C_{60}^+ by much more than the documented scatter of DIB9633 and DIB9577 wavelengths/intensities. It should also be noticed that complexes with helium, experimentally observed by Campbell et al., formed with a high number density of He atoms (10^{15} cm^{-3}) and that temperatures below 8 K were required. Such species have therefore not been postulated to be of any significance for the DIB phenomenon.

It seems that the only astronomically observed parameters that match the laboratory ones relatively well are FWHMs of diffuse bands. They are slightly broader than the laboratory ones for 9577 band, but in general the similarity is satisfactory in most of the observed lines of sight (Table 2).

5 CONCLUSIONS

The results from the observed sample of 19 reddened stars having spectra with easily detectable diffuse bands at 9577 and 9633 Å do not allow us to assign these features to near-IR transitions of C_{60}^+ , and thus to confirm the presence of this cation in translucent interstellar clouds, for the following reasons:

- The ratio of DIB9633 and DIB9577 equivalent widths is variable within a broad range: see Table 2 and, for example, Figs. 7, 9, 10. The resultant mutual correlation is very poor,

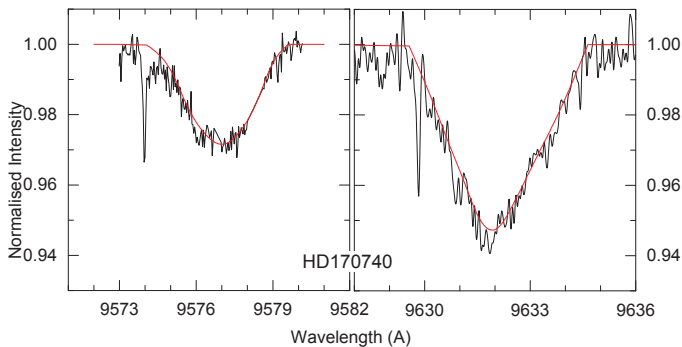


Figure 10. Diffuse bands at 9577 and 9633 Å (corrected profiles, same ordinate scale). The latter is 1.6 times stronger than the former, while the respective ratio, expected for C_{60}^+ , is 0.8! Note that the originally observed intensity ratio, before the subtraction of a stellar MgII contribution, was even greater, as big as 1.9.

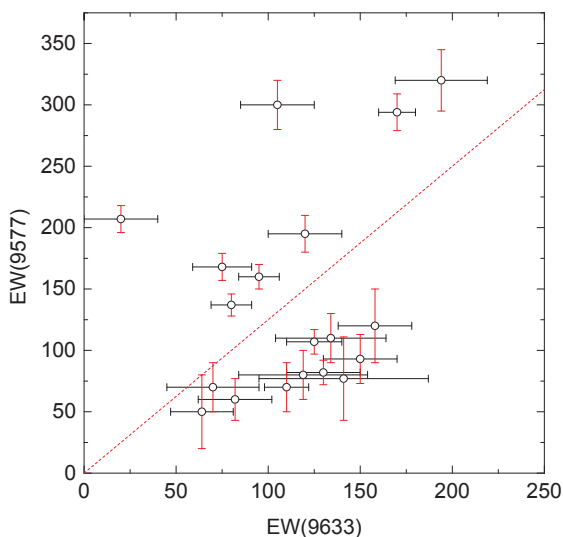


Figure 11. Very poor intensity correlation of 9633 and 9577 Å diffuse bands. Dotted line represents the equivalent width ratio $DIB_{9633}/DIB_{9577}=0.8$. Differences in strength ratios are much bigger than measurement errors.

much worse than within any other pair of reasonably strong DIBs (Fig. 11).

- We have not confirmed the presence of two weaker members of the C_{60}^+ family, expected at 9428 and 9366 Å the former is stronger in laboratory but more difficult to be traced in observations, even though these should appear assuming the validity of experimentally determined intensity ratios.
- The “interstellar” wavelengths of the two strongest DIBs proposed for C_{60}^+ show evident variability, but not in unison, i.e. the distance between DIB9633 and DIB9577 discernibly fluctuates.
- The profile shapes of both diffuse bands are variable. In particular, asymmetric profiles were found in several cases, contrasting with what was reported for gas-phase C_{60}^+ .

In general, the observed very poor correlation of the two discussed DIBs can be explained, together with the variable shapes of DIB profiles, by some blending with other, as yet unresolved diffuse bands. Nevertheless, both the lack of a

firm detection of the two minor bands expected for C_{60}^+ and, for the major candidate bands, the disagreement of central wavelengths with laboratory values need to be addressed in order to defend the recently claimed identification of C_{60}^+ .

Cami et al. (2010) suggested that “the absence of the corresponding spectral features of fullerene cations and anions implies that the fullerenes are in the neutral state”. This remark, formulated in the context of *circumstellar* matter, may prove correct for translucent interstellar clouds also.

ACKNOWLEDGEMENTS

This paper includes data gathered with the VLT and UVES spectrograph, programs 067.C-0281(A), 082.C-0566(A), 092.C-0019(A). Authors acknowledge Dr. H. Linnartz and Dr. R.Kolos for his valuable comments and suggestions. GAG and GV acknowledge the support of Russian Science Foundation (project 14-50-00043, area of focus Exoplanets). VVS acknowledges the Russian Fund for Basic Researches 16-02-01145 (Non-LTE modeling of stellar atmospheres). JK acknowledges the grant 2015/17/B/ST9/03397 of the Polish National Science Center.

REFERENCES

- Berné O., Mulas G., Joblin C., 2013, A&A, 550, L4
 Cami J., Bernard-Salas J., Peeters E., Malek S.E., 2010, Science, 329, 1180
 Campbell E. K., Holz M., Gerlich D., Maier J. P., 2015, Nature, 523, 322
 Campbell E. K., Holz M., Maier J.P., Gerlich D., Walker G.A.H., Bohlender D., 2016, ApJ, 822, 17
 Campbell E. K., Holz M., Maier J. P., 2016a, ApJ, 826, L4
 Castelli F., Kurucz R. L., 2004, Proceedings of the IAU Symp. No 210, Modelling of Stellar Atmospheres, eds. N. Piskunov et al. 2003, poster A20, arXiv:astro-ph/0405087
 Chentsov E.L., 2004, Astronomy Letters, 30, 325
 Foing B. H., Ehrenfreund P., 1994, Nature, 369, 296
 Galazutdinov G.A., Krelowski J., Musaev F. A., Ehrenfreund P., Foing B.H., 2000, MNRAS, 317, 750
 Galazutdinov G.A., Musaev F.A., Krelowski J., Walker G.A.H., 2000, PASP, 112, 648
 Hobbs L. M., York D. G., Thorburn J. A., Snow T. P., Bishof M., Friedman S. D., McCall B. J., Oka T. and 3 coauthors, 2009, ApJ, 705, 32
 Jenniskens P., Mulas G., Porceddu I., Benvenuti P., 1997, A&A, 327, 337
 Krelowski J., Greenberg J.M., 1999, A&A, 346, 199
 Krelowski J., Galazutdinov G.A., Mulas G., Maszewska M., Cecchi-Pestellini C., 2015, MNRAS, 451, 3210
 Kroto H.W., Heath J.R., Obrien S.C., Curl R.F., Smalley R.E., 1985, Nature, 318, 162
 Menzhevitski V.S., Shimanskaya N.N., Shimansky V.V., Kudryavtsev D. O., 2014, Astrophysical Bulletin, 69, 169
 Sakhibullin N.A., 1983, Kazanskaia Gorodskiaia Astronomicheskiaia Observatoriia, Trudy (ISSN 0371-8247), 48, 9
 Sellgren K., Werner, M.W., Ingalls J.G., Smith J.D.T., Carleton T. M., Joblin C., 2010, ApJ, 722, L54
 Smette A., Sana H., Noll S., Horst H., Kausch W., Kimeswenger S., Barden M., Szyszka C. and 5 coauthors, 2015, A&A, 576, A77
 Tkachenko A., Matthews J. M., Aerts C., Pavlovski K., Papics P.I., Zwintz K., Cameron C., Walker G.A.H. and 11 coauthors, 2016, MNRAS, 458, 1964

Tody D., 1986, "The IRAF Data Reduction and Analysis System"
in Proc. SPIE, Instrumentation in Astronomy VI, ed. D.L.
Crawford, 627, 733
Walker G.A.H., Bohlender D. A., Maier J. P., Campbell E. K.,
2015, ApJL, 812, 8

This paper has been typeset from a $\text{\TeX}/\text{\LaTeX}$ file prepared by
the author.